Neutron study of the normal-incommensurate phase transition in K_2ZnCl_4

1990 J. Phys.: Condens. Matter 2 4543

(http://iopscience.iop.org/0953-8984/2/20/001)

J. Phys.: Condens. Matter 2 (1990) 4543–4558. Printed in the UK

Neutron study of the normal–incommensurate phase transition in K_2ZnCl_4

M Quilichini†, P Bernede†, J Lefebvre‡ and P Schweiss§‖

† Laboratoire PMTM, CNRS, Université Paris-Nord, Avenue J B Clément, 93430 Villetaneuse, France

‡ Laboratoire de Dynamique des Cristaux Moléculaires, (UA 801) UFR de Physique, Université de Lille I, 59655 Villeneuve d'Ascq Cédex, France

§ Laboratoire Léon Brillouin, CEN Saclay, 91191 Gif-sur-Yvette Cédex, France

Received 24 July 1989, in final form 12 December 1989

Abstract. The pretransitional fluctuations in the normal paraelectric phase have been studied by quasi-elastic neutron scattering. They are located at the satellite positions of the incommensurate phase. Correlation lengths ξ_i are given and the dynamics is described by a relaxational process. We studied the width of the $\Sigma 2$ phonon (soft in K_2SeO_4) as a function of q and T. We report a structural neutron analysis of the incommensurate phase, which is described by the $P^{Pnma}_{1s\ s}(\alpha 00)$ superspace group. Structural results are connected with dynamic ones to explain the mechanism of the normal–incommensurate phase transition.

1. Introduction

Potassium tetrachlorozincate K_2ZnCl_4 belongs to the extensively studied K_2SeO_4 family, which presents a prototypical sequence of phase transitions. For K_2ZnCl_4, starting from the normal paraelectric orthorhombic high-temperature phase (N) (space group $Pnma$; $b < a < c$), the crystal transforms to an incommensurate phase (INC) as the temperature decreases to $T_i = 290\,°C$. In the INC phase the wavevector of the static modulated distortion is $\boldsymbol{q} = \alpha \boldsymbol{a}^*$ with $\alpha = \frac{1}{3}[1 - \delta(T)]$, where $\boldsymbol{a}^*$ stands for the reciprocal lattice parameter of the normal phase. The incommensurate parameter δ decreases monotonically with decreasing temperature and jumps to zero at the lock-in temperature $T_c = 130\,°C$ (Gesi 1978), where the crystal reaches the commensurate ferroelectric phase (C) (space group $Pn2_1a$; $b < a < c$) with a tripling of the unit cell along the $\boldsymbol{a}$ axis of the N phase. At $T_0 = 140\,K$, K_2ZnCl_4 undergoes another phase transition, and for lower temperature (the low-temperature phase) the symmetry is not known. From a dynamic point of view, the transition N → INC at T_i is known to have a displacive character in K_2SeO_4, a $\Sigma 2$ optic phonon having been shown to soften in the normal phase (Iizumi *et al* 1977). In Rb_2ZnCl_4 and K_2ZnCl_4 an order–disorder mechanism was proposed (Gesi and Iizumi 1984) even though Raman spectroscopists claimed the existence of an amplitude mode (Quilichini *et al* 1982, Sekine *et al* 1986) (a specific excitation of the incommensurate phase within the frame of the soft mode mechanism) in both materials. Even

‖ Permanent address: Kernforschungszentrum Karlsruhe, JNFT 7500 Karlsruhe, and University of Marburg, Institut für Mineralogie, 3550 Marburg, Federal Republic of Germany.

0953-8984/90/204543 + 16 $03.50

if we consider only the K_2SeO_4-type compounds (Rb_2ZnCl_4, K_2ZnCl_4, Rb_2ZnBr_4), the failure to observe soft modes in the normal phases demonstrates differences that prevent a unified origin of the incommensurate instability in these materials. Nevertheless, and following a suggestion by J D Axe (Axe 1986), we think that a way to understand differences and similarities among this limited family is from a structural origin.

In this paper we present quasi-elastic coherent neutron scattering results and a structural study of the incommensurate phase.

We have already resolved the normal high-temperature phase and the lock-in ferroelectric phase. The results obtained have been partly published (Quilichini *et al* 1988, Quilichini 1986). Nevertheless, those presented here together with those of the incommensurate phase allow a complete coherent description of the three phases.

Both inelastic and elastic experiments were performed on single crystals, which were grown from aqueous solution by slow evaporation. Usually the sample shape was a parallelepiped with faces perpendicular to the main directions a, b and c.

The present paper is organised as follows: in section 2 we analyse quasi-elastic and inelastic neutron data; in section 3 we describe the experimental setting and results of neutron diffraction measurements; in section 4 we introduce our superspace approach of the incommensurate phase; finally in section 5, discussion and conclusions are given.

2. Inelastic and quasi-elastic neutron scattering

The quasi-elastic and inelastic neutron scattering experiments were performed on a triple-axis spectrometer (4F1) located on a cold source at the Orphee Reactor (Saclay). All the measurements were carried out in the ($\boldsymbol{a}^*$, $\boldsymbol{b}^*$) scattering plane. We worked using the constant k_i method, with either $k_i = 2.662$ or 1.55 Å^{-1}, which leads to an energy resolution of 0.25 or 0.04 THz, respectively.

The $\Sigma 3$–$\Sigma 2$ mode, soft in K_2SeO_4, was studied in K_2ZnCl_4 around the (0 4 0) Bragg peak within the temperature range of 20 to 330 °C. As already shown (Gesi and Iizumi 1984) the dispersion curve of this mode is nearly temperature-insensitive.

Our data were fitted with a damped harmonic oscillator as the spectral function convolved with the instrumental response plus a background. The damping factor of the oscillator is Γ. As seen from figure 1, Γ does not depend much on T, the $\Gamma(T)$ curve being about the same in the three phases, namely the ferroelectric phase, the incommensurate phase and the paraelectric phase. From figure 1 one sees that Γ increases with increasing value of q. This is puzzling and we have no definite quantitative explanation for this broadening of the phonon linewidth. First we notice that it occurs for values of q that are of the same order as or greater than the one that defines the position of the diffuse scattering, which will be described below. Secondly, we will show in the next section that, when refining structural data in the three phases, we have abnormally large thermal parameters, which are certainly related to some dynamic disorder. The question is this: How is this disorder related to the phonon linewidth? Following a description proposed by Kurzynski and Halawa (1986) we can assume that a coupling exists between a spin variable attached to the $ZnCl_4$ anion and the phonon variable. In ND_4Br it has been shown by Yamada *et al* (1974a, b) that such a coupling can be responsible for the broadening of the phonon mode.

In the limited family of compounds, Rb_2ZnCl_4, Rb_2ZnBr_4 and K_2ZnCl_4, it has been shown that, instead of the phonon softening, a diffuse scattering located on the satellite positions of the incommensurate phase occurs as a pretransitional effect (Andrews and

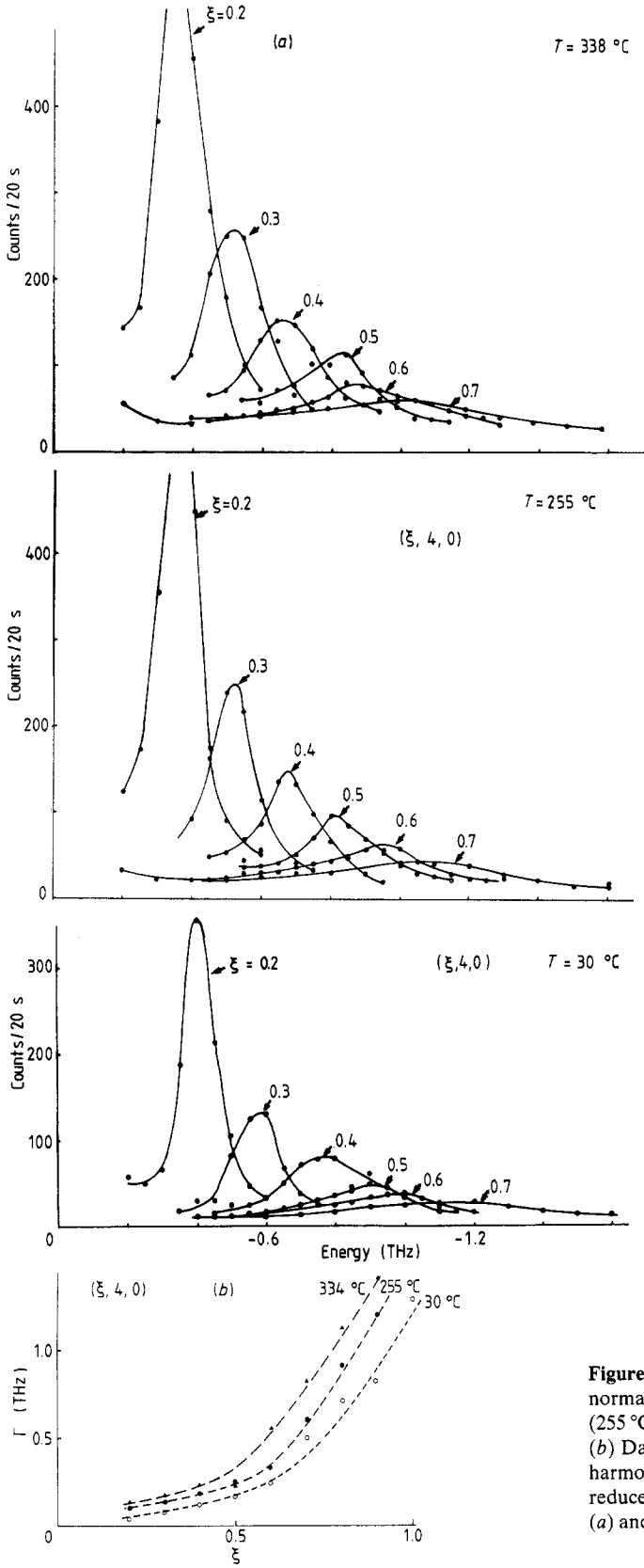

Figure 1. (*a*) Σ3–Σ2 phonon branch in the normal (338 °C), incommensurate (255 °C) and ferroelectric (30 °C) phases. (*b*) Damping coefficient Γ of the damped harmonic oscillator fit as a function of q (in reduced units) in the three phases. In both (*a*) and (*b*), $k_i = 2.662$ Å^{-1}.

Mashiyama 1983, De Pater and van Dijk 1978, Gesi and Iizumi 1984). This diffuse scattering is related to spatial fluctuations of the transition order parameter. We have also studied this diffuse scattering above T_i in K_2ZnCl_4 in a coherent neutron scattering experiment. To give a quantitative description of our experimental results, we use the Ornstein–Zernike theory of fluctuations (Landau and Lifshitz 1980), where the correlation function for the isotropic case reads $kT\exp(-r/\xi)r$, and ξ is the correlation length, and after Fourier transformation the response function has a Lorentzian profile. It is usual to introduce a relaxation time τ; if we use a cluster picture to characterise these precursor effects, τ is the lifetime of a cluster the size of which is ξ. Taking into account the orthorhombic symmetry and the scattering plane used for experiments, following Dorner and Comès (1977) we can write the response function as

$$S(\boldsymbol{Q}, w) = \frac{kT}{\pi} \frac{\xi^2}{1 + \xi_a^2 q_h^2 + \xi_b^2 q_k^2} \frac{\tau}{1 + \tau^2 w^2}$$

where ξ_a and ξ_b are the correlation lengths along $\boldsymbol{a}$ and $\boldsymbol{b}$ respectively; $\xi^2 = \xi_a^2 + \xi_b^2$. The wavevector $\boldsymbol{q} = (q_h, q_k, 0)$ is determined from a satellite position of the incommensurate phase.

Both Q and the energy profiles of this diffuse scattering were studied with T ranging from 285 to 340 °C and around the reciprocal point (1.32, 2, 0), which corresponds to the most intense satellite of the experimental scattering plane. To work out the static part of the spectral function, elastic Q scans were performed in both $\boldsymbol{a}^*$ and $\boldsymbol{b}^*$ directions using an incident k_i equal to 2.662 $Å^{-1}$. The energy resolution (0.25 THz) was large enough to integrate in energy the quasi-elastic scattering. The observed experimental profiles are well fitted with a Lorentzian scattering function convolved with the instrumental response. Its halfwidth at half-maximum (HWHM) L (which is equal to $1/\xi$) is studied as a function of temperature. Figure 2 shows the L^2 temperature dependence, which is proportional to $(T - T_i)$ with $T_i = 293$ °C. This linear behaviour is in agreement with results of the Landau analysis of fluctuations, which leads to ξ^2 proportional to $(T - T_i)^{-1}$. We observed that ξ_a and ξ_b do not decrease steeply as T increases. It is noticed that the crystal deteriorates for temperatures higher than $T = 320$ °C, which prevents good fitting of the data above this temperature. We note also that there is no pronounced anisotropy among these spatial fluctuations.

To determine the relaxation time, energy scans were performed with $k_i = 1.55$ $Å^{-1}$. Profiles are well fitted by a Lorentzian function with a HWHM of 0.04 THz at 300 °C, 0.044 THz at 320 °C and 0.058 THz at 334 °C. This fairly large energy distribution leads to short values of the relaxation time τ ($\tau \simeq 4 \times 10^{-12}$ s at 300 °C).

3. Neutron diffraction measurements

This neutron single-crystal experiment was performed at 180 °C on the 5C2 four-circle diffractometer (Orphee Reactor, Saclay). At this temperature δ is small ($q_\delta \simeq 0.32a^*$) and to collect intensities the following procedures have been used. The recriprocal parameter a^* was divided by a factor of 3. All the reflections (h', k, l) with this reciprocal cell were measured. When h' is a multiple of 3, it is a main reflection; if it is not the case, it is a satellite reflection. The difference between this calculated reflection and the true position of the satellite is negligible. Data were collected with a wavelength of 0.832 Å. The crystal was mounted in a furnace, which allows temperature fluctuations to be kept within ±0.5 °C. Some 4300 main and first-order satellite reflections with $-9 < h < 9$,

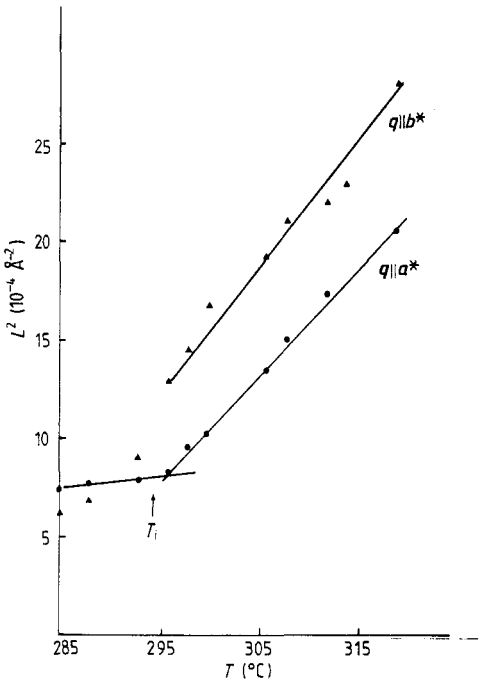

Figure 2. Temperature behaviour of L for q along a^* and b^*. L is the halfwidth at half-maximum of the Lorentzian fitting function. The experimental resolution is of the order of 0.02 Å^{-1}.

$-7 < k < 0$, $0 < l < 13$ were measured using the ω-scan method up to $(\sin\theta)/\lambda = 0.56$ Å^{-1}. The raw data were corrected for background and for the Lorentz factor. Because of the short wavelength, problems arise of contamination of the satellite by main reflections, and about 500 reflections were rejected. The absorption being weak ($\mu = 0.63$ cm^{-1}), the results were not improved by absorption correction. Some 33 first-order satellites were removed because of the possibility of contamination by second-order satellites. (This point will be explained in the following.) Among the 3800 remaining reflections, there were 895 non-equivalent reflections with $I > 3\sigma(I)$ corresponding to 461 main reflections and 434 first-order satellites.

The lattice constants in the incommensurate phase determined from 16 centred single-crystal reflections by least-squares refinement of the orientation matrix are $a = 8.96(3)$ Å, $b = 7.30(1)$ Å, $c = 12.54(3)$ Å.

Standard refinements always lead to large thermal parameters in any of the three phases. As our aim is a reliable description of structures that can support our dynamic studies, we tried, whenever possible, several models.

For the normal phase (Quilichini 1986), where the space group is P*nma* and $Z = 4$, three models have been tested. The first one is based on harmonic anisotropic temperature factors for all atoms, and converges to $R = 0.087$ and $R_w = 0.047$, with

$$R = \frac{\Sigma||F_0| - |F_c||}{\Sigma F_0} \qquad R_w = \frac{\Sigma w(F_0 - |F_c|)^2}{\Sigma w F_0^2}.$$

The weighting scheme was w = unit weight for all reflections.

In the second model, the so-called 'anharmonic' model, the temperature factors of the Cl atoms were expanded up to fourth order using a formalism based on the Gram Charlier expansion of structure factors (Zucker *et al* 1983). This refinement converged

Table 1. Anisotropic temperature parameters ($Å^2 \times 10^4$) in the normal phase at 315 °C. Model 1, P*nma* harmonic potential; model 2, P*nma* anharmonic potential; model 3, P*nma* harmonic split-atom model. They correspond to

$$\exp\left(-2\pi^2 \sum_{ik} U_{ik} h_i k_k a_i^* a_k^*\right) \text{ and with } U_{eq} = \tfrac{1}{3}(U_{11} + U_{22} + U_{33}).$$

	Model	U_{11}	U_{22}	U_{33}	U_{eq}
K(1)	1	860(66)	1668(98)	2154(99)	1561
	2	864(35)	1587(60)	2155(64)	1535
	3	862(42)	1566(77)	2098(81)	1508
K(2)	1	833(58)	1445(95)	872(66)	1050
	2	863(30)	1442(50)	890(40)	1065
	3	822(36)	1435(62)	835(43)	1030
Zn	1	593(26)	734(31)	657(28)	661
	2	614(15)	736(17)	683(16)	677
	3	585(17)	718(20)	659(18)	654
Cl(1)	1	621(22)	2986(73)	1613(40)	1740
	2	700(27)	2558(45)	1625(25)	1628
	3	625(14)	1434(78)	1616(26)	1222
Cl(2)	1	945(30)	3109(66)	883(25)	1645
	2	1077(35)	2671(42)	856(13)	1534
	3	977(20)	1541(77)	857(16)	1125
Cl(3)	1	1786(28)	937(18)	2268(33)	1664
	2	1827(34)	954(19)	2116(30)	1632
	3	1865(160)	940(67)	1356(70)	1375
Cl(4)	3	1305(40)	748(37)	1429(65)	1161

to $R = 0.037$ and $R_w = 0.027$, and the coeficients of the anharmonic temperature factors were then used to calculate the corresponding probability density function (PDF) of the Cl atoms.

Finally in the third description a 'split-atom' model was attempted because of large thermal amplitudes for most atoms. This model was successful when only the Cl atoms were split with an equal occupancy of 0.5, which is required from the symmetry. This refinement converges to $R = 0.041$ and $R_w = 0.027$. The main harmonic parameters obtained with these three models are given in table 1. Except for those of the Zn atoms, these values are anomalously large and very anisotropic.

In the ferroelectric phase (Quilichini *et al* 1988), the space group of which is $Pn2_1a$, a standard refinement using harmonic anisotropic thermal factors (table 2) has shown that they are still large, mainly in the *b* and *c* directions. Starting from the disorder described by the split-atom model in the normal phase, we have calculated the atomic positions in the triple unit cell of the ferroelectric phase, assuming it is ordered. Doing so, we noticed that the orientation of two $ZnCl_4$ units (I and II in Quilichini *et al* 1988) agrees with one of the two positions of the split model, while unit III is still disordered; this explains the larger values of U_{ii} for Cl(2), Cl(6), Cl(9) and Cl(10).

For the incommensurate phase, least-squares calculations based on the main reflections give only what is usually called the 'average' structure. Because it usually has the

Table 2. Thermal parameters ($\times 10^4$) in the ferroelectric phase of K_2ZnCl_4. Estimated standard deviations are in parentheses.

	U_{11}	U_{22}	U_{33}	U_{eq}
K(1)	246(30)	507(40)	535(40)	429
K(2)	320(30)	911(65)	907(65)	713
K(3)	477(40)	826(66)	941(73)	748
K(4)	309(30)	260(30)	498(40)	356
K(5)	284(30)	398(37)	536(40)	406
K(6)	369(27)	289(28)	534(30)	397
Zn(1)	222(14)	261(18)	248(17)	244
Zn(2)	233(16)	222(17)	231(17)	229
Zn(3)	253(14)	316(18)	276(17)	282
Cl(1)	224(9)	565(15)	870(21)	553
Cl(2)	201(9)	596(16)	905(21)	567
Cl(3)	264(9)	417(16)	417(22)	366
Cl(4)	311(14)	303(12)	676(15)	430
Cl(5)	460(14)	330(12)	523(15)	437
Cl(6)	359(12)	292(12)	1456(32)	702
Cl(7)	338(10)	670(16)	310(12)	439
Cl(8)	650(15)	430(12)	325(13)	468
Cl(9)	834(18)	939(23)	324(14)	699
Cl(10)	529(14)	1031(24)	482(16)	681
Cl(11)	502(13)	543(14)	348(13)	464
Cl(12)	530(13)	513(14)	412(15)	485

same space group as the normal phase, it gives a rough description that is easy to compare with this phase. Here we propose in table 3 results of such calculations done using either P*nma* space group symmetry, non-split ($R = 0.11$, $R_w = 0.11$) and split-atom models ($R = 0.09$, $R_w = 0.09$), or $Pn2_1a$ space group ($R = 0.08$, $R_w = 0.047$). As expected, the thermal parameters are smaller in this phase than in the N phase except for U_{22} of K(1), K(2), Cl(1), Cl(2) and U_{33} of Cl(3), Cl(4). Table 4 summarises the atomic fractional coordinates obtained for each model and at temperature 180 °C in the incommensurate phase and 315 °C in the normal phase.

Because anharmonic temperature factors (thermal motion) and split positions (disorder) are mathematically equivalent in describing nuclear densities, we cannot distinguish between ordered (dynamic disorder due to thermal vibrations only) and disordered structures (in addition to thermal vibrations, static deviations form the crystal symmetry) and we do not have additional arguments to decide which is the more realistic description.

4. Superspace symmetry

As pointed out in the introduction, the superspace description is the only appropriate one for the incommensurate phase.

Table 3. Anisotropic temperature parameters ($Å^2 \times 10^4$) in the incommensurate phase. Model 1, P*nma* average structure; model 2, P*nma* split model; model 3, P$n2_1a$ average structure; model 4, $P^{Pnma}_{Is\ s}$ supergroup.

	Model	U_{11}	U_{22}	U_{33}	U_{eq}
K(1)	1	539(73)	1798(198)	1340(148)	1226
	2	629(40)	1364(62)	1273(60)	1088
	3	562(64)	530(94)	1398(135)	830
	4	542(40)	1086(93)	1291(79)	973
K(2)	1	587(68)	1185(111)	539(66)	770
	2	561(32)	1142(48)	550(34)	751
	3	589(66)	1292(132)	634(72)	838
	4	558(37)	698(61)	596(39)	617
Zn	1	351(27)	596(36)	453(32)	467
	2	358(15)	529(16)	434(16)	440
	3	364(26)	567(41)	472(32)	467
	4	365(16)	365(21)	425(18)	385
Cl(1)	1	370(24)	3517(147)	918(41)	1602
	2	405(15)	963(43)	950(13)	773
	3	363(22)	3632(166)	929(40)	1641
	4	347(12)	709(38)	935(22)	664
Cl(2)	1	633(33)	3938(164)	541(31)	1704
	2	651(42)	1228(28)	501(35)	793
	3	649(31)	3899(168)	534(29)	1694
	4	619(17)	796(39)	528(16)	648
Cl(3)	1	1659(49)	669(23)	2415(69)	1581
	2	1227(29)	604(23)	891(34)	907
	3	1514(95)	776(59)	2405(123)	1565
	4	732(19)	594(13)	828(25)	718
Cl(4)	2	843(28)	494(23)	962(34)	766
	3	1762(136)	622(49)	2050(187)	1491

In such a phase the diffraction pattern consists of sharp peaks, which can all be indexed with four indices on a set of four vectors $\boldsymbol{b}_i$. This leads to

$$\boldsymbol{Q} = h_1\boldsymbol{b}_1 + h_2\boldsymbol{b}_2 + h_3\boldsymbol{b}_3 + h_4\boldsymbol{b}_4$$

with

$$\boldsymbol{b}_4 = q_1\boldsymbol{b}_1 + q_2\boldsymbol{b}_2 + q_3\boldsymbol{b}_3.$$

The main characteristic of this diffraction image is that it shows a very conspicuous three-dimensional lattice B (De Wolff 1974) among the points $(h_1h_2h_3h_4)$. These peaks are the 'main reflections' and they correspond to $h_4 = 0$ with a proper choice of $\boldsymbol{b}_i$. When going through the transition phase temperature T_i, these reflections remain, whereas the 'satellites' having $h_4 \neq 0$ disappear. A reasonable choice for B appears to be the reciprocal lattice of the normal phase based on $\boldsymbol{a}^*, \boldsymbol{b}^*, \boldsymbol{c}^*$.

Then the already mentioned 'average structure' is identical to the direct lattice A reciprocal to B. To recover the translational symmetry property, the superspace approach introduces a four-dimensional space B' so that the satellites are projections

Table 4. Atomic fractional coordinates ($\times 10^4$) of K_2ZnCl_4 in the incommensurate phase ($T = 180$ °C, 'average' structure) and in the normal phase. Model 1, P*nma* space group non-split model; model 2, P*nma* space group split-atom model; model 3, P$n2_1a$ space group.

	180 °C				315 °C			
	Model	*x/a*	*y/b*	*z/c*	Model	*x/a*	*y/b*	*z/c*
K(1)	1	6339(16)	2500	4143(18)	1	6355(11)	2500	4114(12)
	2	6327(7)	2500	4145(7)	2	6356(7)	2500	4131(8)
	3	6354(15)	2874(26)	4161(17)				
K(2)	1	4960(13)	2500	8126(9)	1	4942(10)	2500	8129(6)
	2	4949(6)	2500	8126(4)	2	4935(4)	2500	8129(4)
	3	4951(13)	2462(52)	8125(9)				
Zn	1	2190(6)	2500	4188(5)	1	2195(4)	2500	4205(4)
	2	2179(3)	2500	4194(3)	2	2194(3)	2500	4206(2)
	3	2191(6)	2500	4191(5)				
Cl(1)	1	9748(6)	2500	4342(5)	1	9768(4)	2500	4288(4)
	2	9748(3)	3068(4)	4346(2)	2	9771(2)	2990(10)	4295(2)
	3	9749(5)	2606(60)	4348(5)				
Cl(2)	1	3309(6)	2500	5782(5)	1	3231(4)	2500	5797(4)
	2	3307(3)	1903(4)	5777(2)	2	3231(2)	2011(9)	5798(2)
	3	3310(6)	2535(63)	5782(4)				
Cl(3)	1	3028(7)	55(7)	3325(6)	1	3063(4)	55(5)	3368(6)
	2	2753(6)	184(11)	3064(4)	2	2887(18)	204(23)	3143(7)
	3	3052(16)	70(25)	3421(15)				
Cl(4)	2	3241(5)	5058(10)	3557(3)	2	3202(17)	5070(22)	3571(7)
	3	3014(19)	4840(25)	3238(16)				

along $(\boldsymbol{q} + \boldsymbol{e}_4)$ onto the 3D space B of lattice points of B'. B' is based on vectors $\boldsymbol{b}_i'$ with $\boldsymbol{b}_1' = \boldsymbol{a}^*, \boldsymbol{b}_2' = \boldsymbol{b}^*, \boldsymbol{b}_3' = \boldsymbol{c}^*, \boldsymbol{b}_4' = \boldsymbol{q} + \boldsymbol{e}_4$; here $\boldsymbol{e}_4$ is a unit vector perpendicular to R_3. The 4D direct lattice A' reciprocal to B' is based on vectors $\boldsymbol{a}_i'$ such as $\boldsymbol{a}_i' = \boldsymbol{a}_i - \boldsymbol{q} \cdot \boldsymbol{e}_4$ $(i = 1, 2, 3)$, $\boldsymbol{a}_4' = \boldsymbol{e}_4$ and $\boldsymbol{a}_i' \cdot \boldsymbol{b}_j' = \delta_{ij}$. In A' one introduces a periodic function $\rho'(\boldsymbol{r}, t)$, which has the translation periodicity of A'. From the construction of ρ' it comes out that the real 3D density function of the crystal $\rho(r)$ is nothing other than the section of ρ' by the hyperplane R_3 perpendicular to $\boldsymbol{e}_4$. If x_i $(i = 1, \ldots, 4)$ are coordinates in A', then $x_4 = q_1x_1 + q_2x_2 + q_3x_3$. A new coordinate $t = x_4 - q_1x_1 - q_2x_2 - q_3x_3$ has been introduced in A' that restores the translation symmetry and expresses formally that in a real incommensurate structure the phase is arbitrary. For a displacive modulated crystal, the atomic positions in the 4D lattice for the atom μ are

$$x_i^\mu(\bar{x}_4^\mu) = \bar{x}_i^\mu + u_i^\mu(\bar{x}_4^\mu) \qquad i = 1, \ldots, 4$$

where $\bar{x}_i^\mu$ is the averaged position of the atom in the basic structure A and $\bar{x}_4^\mu = \boldsymbol{q} \cdot \bar{\boldsymbol{x}}^\mu + t$.

The modulation functions $\boldsymbol{u}^\mu$ attached to each atom are generally different for the different atoms in the unit cell of the basic structure, but with the same vector $\boldsymbol{q}$; they are expanded in Fourier series as

Table 5. Space-group operations of $P^{Pnma}_{1s\,s}(\alpha 00)$, $\{R, \varepsilon|v, \tau\}$. R, v, ε and τ are given for each operation.

$\begin{pmatrix} E \\ 1 \end{pmatrix}$	$\begin{pmatrix} 1 & 0 & 0 \\ 0 & 1 & 0 \\ 0 & 0 & 1 \end{pmatrix}$	$\begin{pmatrix} 0 \\ 0 \\ 0 \end{pmatrix}$	1	0
$\begin{pmatrix} n \\ \bar{1} \end{pmatrix}_a$	$\begin{pmatrix} -1 & 0 & 0 \\ 0 & 1 & 0 \\ 0 & 0 & 1 \end{pmatrix}$	$\begin{pmatrix} \frac{1}{2} \\ \frac{1}{2} \\ \frac{1}{2} \end{pmatrix}$	-1	0
$\begin{pmatrix} 2_1 \\ \bar{1} \end{pmatrix}_b$	$\begin{pmatrix} -1 & 0 & 0 \\ 0 & 1 & 0 \\ 0 & 0 & -1 \end{pmatrix}$	$\begin{pmatrix} 0 \\ \frac{1}{2} \\ 0 \end{pmatrix}$	-1	1/2
$\begin{pmatrix} a \\ s \end{pmatrix}_c$	$\begin{pmatrix} 1 & 0 & 0 \\ 0 & 1 & 0 \\ 0 & 0 & 1 \end{pmatrix}$	$\begin{pmatrix} \frac{1}{2} \\ 0 \\ \frac{1}{2} \end{pmatrix}$	1	1/2
$\begin{pmatrix} m \\ s \end{pmatrix}_b$	$\begin{pmatrix} 1 & 0 & 0 \\ 0 & -1 & 0 \\ 0 & 0 & 1 \end{pmatrix}$	$\begin{pmatrix} 0 \\ \frac{1}{2} \\ 0 \end{pmatrix}$	1	1/2
$\begin{pmatrix} 2_1 \\ 1 \end{pmatrix}_a$	$\begin{pmatrix} 1 & 0 & 0 \\ 0 & -1 & 0 \\ 0 & 0 & -1 \end{pmatrix}$	$\begin{pmatrix} \frac{1}{2} \\ \frac{1}{2} \\ \frac{1}{2} \end{pmatrix}$	1	0
$\begin{pmatrix} 2_1 \\ \bar{1} \end{pmatrix}_c$	$\begin{pmatrix} -1 & 0 & 0 \\ 0 & -1 & 0 \\ 0 & 0 & -1 \end{pmatrix}$	$\begin{pmatrix} \frac{1}{2} \\ 0 \\ \frac{1}{2} \end{pmatrix}$	-1	1/2
$\begin{pmatrix} i \\ \bar{1} \end{pmatrix}$	$\begin{pmatrix} -1 & 0 & 0 \\ 0 & -1 & 0 \\ 0 & 0 & -1 \end{pmatrix}$	$\begin{pmatrix} 0 \\ 0 \\ 0 \end{pmatrix}$	-1	0

$$x_i^\mu(\bar{x}_4^\mu) = \sum_{m=1}^{\infty} [a_{m,i}^\mu \cos(2\pi m \bar{x}_4^\mu) + b_{m,i}^\mu \sin(2\pi m \bar{x}_4^\mu)] \qquad i = 1, \ldots, 4.$$

Because only first-order satellites have been measured, the previous expansion has been limited to $m = 1$.

We can write

$$a_{1,i}^\mu = a_i^\mu \qquad b_{1,i}^\mu = b_i^\mu$$

and

$$a_4^\mu = \sum_{i=1}^{3} q_i a_i^\mu \qquad b_4^\mu = \sum_{i=1}^{3} q_i b_i^\mu.$$

Using the four-indices notation, the following systematic absences have been observed in K_2ZnCl_4:

(i) $(h, k, 0, m)$, $h + m = 2n + 1$.
(ii) $(0, k, l, 0)$, $k + l = 2n + 1$.
(iii) For $(h, 0, l, m)$ reflections, most first-order satellites have their intensity equal to zero. Nevertheless, about 10 of them have a small, but non-zero, intensity.

A first calculation has been made with the superspace group $P^{Pn\,2n\,a}_{1\,1\,s})(\alpha 00)$ corresponding to a non-systematic extinction for these reflections. The agreement was very poor and, in particular, the calculated structure factor for these reflections was poor. In fact, this intensity seems to come from the second-order satellite $(h \pm 0.36, 0, 1)$ when

the first-order satellite is at $(h \pm 0.32, 0, 1)$. This point will be discussed in the following and it can be concluded on the existence of a systematic extinction for $(h, 0, l, m)$ reflections when $m = 2n + 1$. This gives, following De Wolff *et al* (1981), the $P^{Pnma}_{1ss}(\alpha 00)$ superspace group. In table 5 we have summed up how symmetry operations $\{R, \varepsilon | \boldsymbol{v}, \tau\}$ act on atomic coordinates; $\{R, \boldsymbol{v}\}$ is the usual 3D space group operation, while $\{\varepsilon, \tau\}$ transforms the internal t coordinate as $t' = \varepsilon t - \boldsymbol{q} \cdot \boldsymbol{v} + \tau$. If we write the position of the atom μ in the nth unit cell as

$$\boldsymbol{R}^{n,\mu} = \bar{\boldsymbol{R}}^{n,\mu} + \boldsymbol{a}^{\mu} \cos[2\pi(\boldsymbol{q} \cdot \bar{\boldsymbol{R}}^{n,\mu} + t)] + \boldsymbol{b}^{\mu} \sin[2\pi(\boldsymbol{q} \cdot \bar{\boldsymbol{R}}^{n,\mu} + t)]$$

with $\bar{\boldsymbol{R}}^{n,\mu} = \boldsymbol{R}^{n} + \bar{\boldsymbol{x}}^{\mu}$, the structure factor is given by

$$F(\boldsymbol{Q}) = \sum_{n} \sum_{\mu} B^{\mu} \exp(2i\pi \boldsymbol{Q} \cdot \boldsymbol{R}^{n,\mu})$$

B^{μ} being the neutron scattering length of the atom μ. Straightforward calculations lead to

$$F(\boldsymbol{Q}) = \sum_{\mu,p,p'} B^{\mu} (i)^{p'} \exp(2i\pi \bar{\boldsymbol{x}} \cdot \bar{\tau}) J_{p'}(2\pi \boldsymbol{Q} \cdot \boldsymbol{a}^{\mu}) J_{p}(2\pi \boldsymbol{Q} \cdot \boldsymbol{b}^{\mu}) \exp[2i\pi(p + p')t]$$

with

$$\boldsymbol{Q} = \boldsymbol{\tau} - (p + p')\boldsymbol{q} = [h - (p' + p)\alpha]\boldsymbol{a}^* + k\boldsymbol{b}^* + l\boldsymbol{c}^*$$

($\boldsymbol{\tau}$ is a vector of the reciprocal lattice B). J_p and $J_{p'}$ are Bessel functions of order p and p' respectively.

Main reflections correspond to $p + p' = 0$, while satellites of order m ($m = -(p + p')$) are given by

$$F_m(\boldsymbol{Q}) = F(h, k, l, m)$$

$$= (-1)^m N \exp(-2\pi^2 m^2 \langle t^2 \rangle) \sum_{\mu} W^{\mu}(\boldsymbol{Q}) B^{\mu} \exp(2i\pi \boldsymbol{\tau} \cdot \boldsymbol{x}^{\mu})$$

$$\times \sum_{p} (-i)^p J_p(2\pi \boldsymbol{Q} \cdot \boldsymbol{a}^{\mu}) J_{m+p}(2\pi \boldsymbol{Q} \cdot \boldsymbol{b}^{\mu})$$

where we used $J_{-m-p}(x) = (-1)^{m+p} J_{m+p}(x)$ and the usual temperature factor $W^{\mu}(\boldsymbol{Q})$ has been introduced,

$$W^{\mu}(\boldsymbol{Q}) = \exp\left(-2\pi^2 \sum_{ij} U^{\mu}_{ij} Q_i Q_j\right).$$

Our refinements in P^{Pnma}_{1ss} superspace group were based on

$$F_0(\boldsymbol{Q}) = F_0(\boldsymbol{\tau}) = N \sum B^{\mu} W^{\mu}(\boldsymbol{Q}) \exp(2i\pi \boldsymbol{\tau} \cdot \bar{\boldsymbol{x}}^{\mu})$$

$$\times [J_0(a\mu) J_0(b\mu) - 2J_2(a\mu) J_2(b\mu) + \ldots +]$$

$$a\mu = 2\pi \boldsymbol{Q} \cdot \boldsymbol{a}^{\mu} \qquad b\mu = 2\pi \boldsymbol{Q} \cdot \boldsymbol{b}^{\mu}$$

$$F_{\pm 1}(\boldsymbol{Q}) = 2 \exp(-2\pi^2 \langle t \rangle^2) N \sum B^{\mu} W^{\mu}(\boldsymbol{Q}) \exp(2\pi i \boldsymbol{\tau} \cdot \bar{\boldsymbol{x}}^{\mu})$$

$$\times \{[J_1(a\mu) J_1(b\mu) - 3J_3(a\mu) J_3(b\mu)](\mp 1/a\mu + i/b\mu) + \ldots\}$$

for main and first order satellite reflections, respectively. As has been seen previously, first-order satellites can be contaminated by second-order ones. In order to prevent this

effect, the following procedure has been used. Refinements have been made with all first-order satellites such as $I > 3\sigma(I)$. Then, for these reflections $(h, k, l, \pm 1)$, the structure factor of the second-order neighbour satellites $(h \pm 1, k, l, \mp 2)$ was calculated using parameters of the previous refinement. When the increase of the structure factor was greater than 20%, the reflection was rejected and the refinement was repeated. Using this procedure, 33 first-order satellites were removed. The final R (R_w) factors are 0.071 (0.071), 0.111 (0.128) and 0.085 (0.085) for main reflections, first-order satellites and total reflections, respectively. Atomic positions, Fourier coefficients of the modulation functions and thermal parameters are given in tables 3 and 6. The calculated phase factor $\langle t^2 \rangle$ is 0.0098(6), which leads to an overall factor of 0.824 for first-order satellites.

Even though the R factors are not much improved, data are better described with this refinement. One can notice that Cl(1) and Cl(2) atoms display the largest amplitude of modulation functions along $\boldsymbol{b}$, while the amplitudes for Cl(3) (Cl(4)) atoms are small along $\boldsymbol{b}$ and large along $\boldsymbol{a}$ and $\boldsymbol{c}$. From table 3 one can compare the main U_{ii} values calculated with each method of refinement. For K(1), K(2), Zn, Cl(1), Cl(2) one sees that U_{11} and U_{33} do not depend much on the model, while U_{22} is very sensitive to it. This reflects the importance of taking modulation functions into account, as was already obvious in writing the structure factor for the main reflections.

As in Rb_2ZnCl_4 and Rb_2ZnBr_4 the thermal parameters of one of the two cations (here K(1)) are much larger than those of the second and even of all other atoms of the unit cell. They remain large in the ferroelectric phase. Finally the large values of the thermal parameters have partly to be related to the high temperature range where the incommensurate and normal phases are observed.

Table 6. Atomic fractional coordinates of the basic structure ($\times 10^4$), Fourier coefficients of the modulation functions ($\times 10^4$), amplitude ($A_i \times 10^4$) and phase ϕ_i of the modulation functions for K_2ZnCl_4 in the $P^{Pnma}_{1s\,s}$ supergroup.

	i	x_i	b_i	a_i	A_i	ϕ_i
K(1)	1	6345(9)	0	0		
	2	2500	−262(32)	311(32)	407	0.888
	3	4153(9)	0	0		
K(2)	1	4963(7)	0	0		
	2	2500	−362(22)	−149(26)	391	0.688
	3	8127(6)	0	0		
Zn	1	2188(4)	0	0		
	2	2500	−173(11)	−173(10)	245	0.625
	3	4190(3)	0	0		
Cl(1)	1	−2490(3)	0	0		
	2	2500	−866(8)	−62(15)	868	0.739
	3	4353(3)	0	0		
Cl(2)	1	3311(3)	0	0		
	2	2500	−51(15)	−914(8)	915	0.509
	3	5781(2)	0	0		
Cl(3)	1	3012(3)	211(6)	−345(5)	404	0.413
	2	57(4)	−107(8)	123(7)	163	0.886
	3	3314(2)	15(5)	−376(3)	376	0.494

Table 7. Bond lengths (Å) and angles (deg) of $ZnCl_4$ groups at 180 °C.

			$P^{Pnma}_{1s\,s}$		
	*Pnma**	$Pn2_1a$*	Min.	Max.	$\Delta d/d_{mean}$ (%)
Zn–Cl(1)	2.197(8)	2.198(7)	2.193	2.281	3.9
Zn–Cl(2)	2.236(8)	2.233(8)	2.234	2.312	3.4
Zn–Cl(3)	2.219(6)	2.247(15)	2.219	2.316	4.3
Zn–Cl(4)		2.211(15)			
Cl(1)ZnCl(2)	111.6(4)	111.5(4)			
Cl(1)ZnCl(3)	112.3(2)	114.2(10)			
Cl(2)ZnCl(3)	106.5(3)	103.9(12)			
Cl(3)ZnCl(4)	107.1(4)	107.4(4)			
Cl(1)ZnCl(4)		110.6(10)			
Cl(2)ZnCl(4)		108.9(12)			

* Average structure.

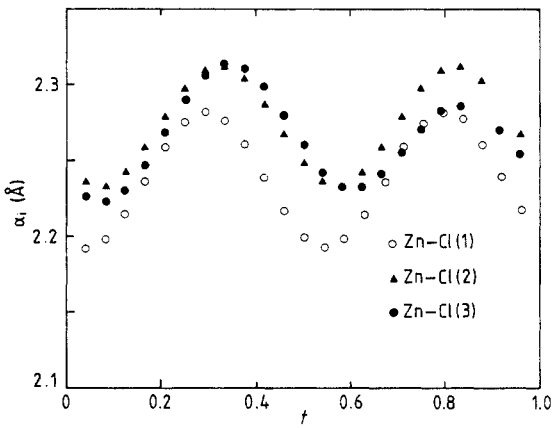

Figure 3. Zn–Cl(i) bond lengths ($i = 1, 2, 3$) as a function of the phase t in the incommensurate phase.

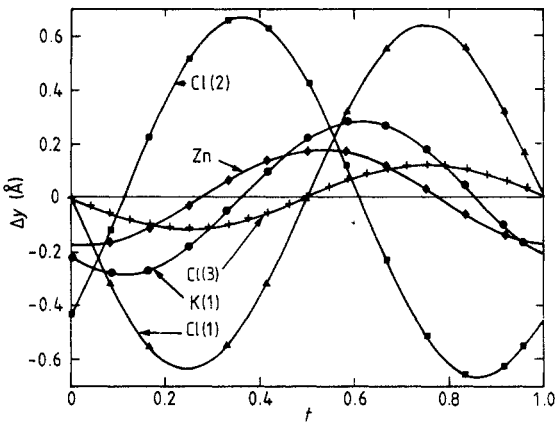

Figure 4. Displacements along b of atoms K(1), K(2), Zn, Cl(1), Cl(2) and Cl(3) from their mean position in the basic structure.

Table 7 sums up bond lengths and angles of $ZnCl_4$ groups calculated with each refinement. Values obtained in the P*nma* space group are comparable to those of the normal phase, showing that these groups are not distorted at the transition. In figure 3 we picture the Zn–Cl(i) bond lengths as a function of phase t, while in figure 4 the deviation from the mean position in the basic structure is also given as a function of t.

We should mention here that we have tried the same analysis of the modulated ferroelectric phase where superlattice reflections appear for $\boldsymbol{q}_c = \boldsymbol{a}^*/3$ for which the space group is P$n2_1a$. The observed systematic extinctions written in the four-indices notation and using the normal phase lattice, $(0, k, l, 0)$ with $(k + l)$ odd, $(0, k, 0, 0)$ with k odd, $(h, k, 0, m)$ with $(3h + m)$ odd, lead to the superspace group $P^{Pn2_1a\,a}_{1\,1\,s}$.

The structure factor is written as in the incommensurate phase except that the term $\exp[2\pi i(p + p')t]$ does not exist any more. The results obtained using the same approximations as before are not satisfactory enough to be kept. The main difficulty for such a treatment lies in the fact that one unit is still disordered in this phase, which prevents a good simultaneous evaluation of thermal parameters and amplitude of modulation.

5. Discussion and conclusions

We have shown that the incommensurate phase of K_2ZnCl_4 is described by the same superspace group $P^{Pnma}_{1s\,s}(\alpha 00)$ as the incommensurate phases of K_2SeO_4 (Yamada and Ikeda 1983), Rb_2ZnCl_4 (Hedoux *et al* 1989) and the room-temperature phase of Rb_2ZnBr_4 (Hogervorst and Helmholdt 1988).

From the preceding sections it is shown that satellite reflections and pretransitional quasi-elastic scattering are indeed the signature of the transition at T_i.

In the normal phase the diffuse scattering described in section 2 gives the q dependence of the static order parameter susceptibility. Such diffuse scattering has also been shown in Rb_2ZnCl_4 above T_i via x-ray investigation (Andrews and Mashiyama 1983) and in Rb_2ZnBr_4 with a neutron experiment (de Pater *et al* 1978) where the experimental results are quite comparable. In the three compounds the diffuse profile is well analysed by a Lorentzian function leading to correlation lengths ξ_a and ξ_b that do not exhibit a pronounced anisotropy and diverge on approaching T_i from above. The present study also gives τ (at the wavevector $\boldsymbol{q}_\delta$) calculated from an analysis of the energy profile of this diffuse scattering. For temperatures at least 10 °C above T_i the relaxation time is of the same order of magnitude as the lattice vibrational timescale. Measurements at higher resolution would be needed to obtain $\tau(q_\delta)$ for temperatures close to T_i and to work out the dispersion of τ with q.

It can be said that any phase transition in this family is due to change of the orientational ordering of $ZnCl_4$ groups accompanied by cationic displacements.

Two complementary statistical models have been proposed to explain the phase diagram features of A_2MX_4-type materials. The first one is the 'extended antiferroelectric interaction Ising' model discussed by Yamada and Hamaya (1983) and the second one is a double Ising model with nearest-neighbour antisymmetric interaction by Kurzynski *et al* (1989). In their model Kurzynski and Halawa (1986) introduced two Ising spin variables ($\sigma\eta$), which describe the different orientations of the $ZnCl_4$ group. Within each of the four $\sigma\eta$ states there should be three substrates which correspond to some tilting (described by the Ising μ variable) of the tetrahedra. Within this description the normal paraelectric phase is ordered in σ (σ describes the positions of the tetrahedron

with one of the apices up or down the pseudo-hexagonal a axis) and the normal incommensurate phase transition would then correspond to the partial (one of three anions is still disordered) ordering of η (η describes the rotation of the anion about the a axis to the right or to the left) while ordering in tilt is not achieved. This is supported by our diffraction results presented in section 3, which demonstrate the existence of large thermal parameters in the three phases (ferroelectric, incommensurate and paraelectric) and the disorder of one $ZnCl_4$ group every three groups in the ferroelectric phase. Then in the normal phase the broadening of the $\Sigma 2$ phonon mode described in section 2 could be due to a complex coupling of this mode with the η and μ variables, while the observed diffuse scattering would be related to short-range ordering in η (here the variable η corresponds to the τ variable in Kurzynski and Halawa (1986)).

In K_2SeO_4 this same transition at T_i is nearly entirely displacive (Iizumi *et al* 1977). In this latter compound the $\Sigma 2$ mode appears to be a complex motion, which involves translational motions in the b direction ($b < a < c$) of all constituents and librational motions of the SeO_4 groups around the c direction, the amplitude of the translational components being much larger than the rotational ones. Above and close to T_i the inelastic neutron data also suggested the presence of a relaxational motion. To reconcile K_2ZnCl_4 and K_2SeO_4 results we have to assume that in these A_2MX_4 compounds the mechanism of the transition at T_i involves a coupling between the $\Sigma 2$ phonon mode and a relaxational mode connected to the reorientation of MX_4 groups. A typical example of such a coupled system is seen in ND_4Br (Yamada *et al* 1974a, b) and it has been shown that the dynamic behaviour depends strongly upon the ratio of the phonon frequency ω_0 and the flipping frequency τ_0^{-1} of the pseudo-spin variable, which specifies the orientation of the MX_4 group. If $\tau_0^{-1} \ll \omega_0$ (slow relaxation) the critical behaviour is mainly seen in the central component of the phonon response, while for $\tau_0^{-1} \gg \omega_0$ it appears in the critical softening of the phonon. Then K_2SeO_4 would correspond to the fast relaxation regime while K_2ZnCl_4 would be characterised by a slow relaxation regime.

This unique mechanism would then explain why the atomic displacement pattern of the INC phase is described by the same superspace in every compound.

References

Andrews S R and Mashiyama H 1983 *J. Phys. C: Solid State Phys.* **16** 4985–96

Axe J D 1986 *Incommensurate Phases in Dielectrics* vol II *(Modern Problems in Condensed Matter Sciences)* ed R Blinc and A P Levanuyk (Amsterdam: North-Holland) p 1

De Pater C J and van Dijk C 1978 *Phys Rev.* B 1281–93

De Wolfe P M 1974 *Acta Crystallogr.* A **30** 777–85

De Wolfe P M, Janssen T and Janner A 1981 *Acta Crystallogr.* A **37** 625–36

Dorner B and Comès R 1977 *Dynamics of Solids and Liquids by Neutron Scattering* ed S W Lovesey and T Springer (Berlin: Springer)

Gesi K 1978 *J. Phys. Soc. Japan* **45** 1431–2

Gesi K and Iizumi M 1984 *J. Phys. Soc. Japan* **53** 4271–8

Hedoux A, Grebille D, Jaud J and Godefroy G 1989 *Acta Crystallogr.* B **45** 370–8

Hogervorst A C R and Helmholdt R B 1988 *Acta Crystallogr.* B **44** 120–8

Iizumi M, Axe J D, Shirane G and Shimaoka K 1977 *Phys. Rev.* B **15** 4392–411

Kurzynski M and Halawa M 1986 *Phys. Rev.* B **34** 4846–53

Kurzynski M, Ossowski M and Bartowiak M 1989 *Ferroelectrics* submitted

Landau L D and Lifshitz E M 1980 *Statistical Physics* vol 1 (Oxford: Pergamon)

Quilichini M 1986 *Incommensurate Crystals, Liquid Crystals and Quasi-Crystals (NATO ASI Series)* ed J F Scott and N Clark (New York: Plenum) pp 127–38

Quilichini M, Heger G and Schweiss P 1988 *Ferroelectrics* **79** 117–20
Quilichini M, Mathieu J P, Lepostellec M and Toupry N 1982 *J. Physique* **43** 787–93
Quilichini M and Pannetier J 1983 *Acta Crystallogr.* B **39** 657–63
Sekine T, Takayama M, Uchinokura K and Matsuura E 1986 *J. Phys. Soc. Japan* **55** 3903–17
Yamada N and Ikeda T 1983 *J. Phys. Soc. Japan* **53** 2555–64
Yamada Y and Hamaya N 1983 *J. Phys. Soc. Japan* **52** 3466–74
Yamada Y, Noda Y, Axe J D and Shirane G 1974a *Phys. Rev.* B **9** 4429–38
Yamada Y, Takatera H and Huber D L 1974b *J. Phys. Soc. Japan* **36** 641–8
Zucker U H, Perenthaler E, Kuhs W F, Bachmann R and Schulz H 1983 *J. Appl. Crystallogr.* **16** 358